AiMT

Advances in Military Technology
Vol. 14, No. 2 **(2019)**, pp. 347-361
ISSN 1802-2308, eISSN 2533-4123
DOI 10.3849/aimt.01285

Magnetohydrodynamic Model of Electric Arc during Contact Opening

M. Mačák*, P. Vyroubal and J. Maxa

Department of Electrical and Electronic Technology, Faculty of Electrical Engineering and Communication, Brno University of Technology, Czech Republic

The manuscript was received on 17 January 2019 and was accepted after revision for publication on 11 November 2019.

Abstract:

A numerical model of an electric arc based on Magnetohydrodynamics Theory was investigated, adjusted and implemented as a user-defined model into ANSYS FLUENT. The goal of this model was to simultaneously calculate electric and magnetic fields, which is not possible with built-in ANSYS MHD model. This custom model was then applied on a problem which described opening of contacts between which an electric arc was created. The development of the arc was investigated by its temperature field. A comparison of built-in and presented model was carried out.

Keywords:

ANSYS FLUENT, CFD, magnetohydrodynamics, plasma

1. Introduction

Magnetohydrodynamics (MHD) is used to describe a flow of electrically conducting fluids (molten metals, strong electrolytes and plasmas) in the presence of an electromagnetic field. In terms of a plasma MHD, certain assumptions are taken into account, which will be described later in the text. This simplifies the mathematical model, but it reduces the application range just to non-relativistic flows. Still, plasma phenomena are quite complex, as they consist of fluid dynamics, thermodynamics, chemical reactions, electromagnetics and sometimes they include the movement of mechanical parts.

Because of these complex mechanisms, many researchers rely on experiments to investigate the plasma phenomenon. However, it is sometimes difficult to measure certain parameters such as a gas velocity or a temperature distribution or an induced magnetic field. It becomes even more complicated when the plasma is enclosed, and a high-speed camera cannot be used. As these experiments are usually expensive and

* *Corresponding author: Department of Electrical and Electronic Technology, Faculty of Electrical Engineering and Communication, Brno University of Technology, Czech Republic. E-mail: macak@feec.vutbr.cz*

time consuming, it is favourable to use numerical simulations as a complement or even as an alternative method. With the use of numerical simulations, it is possible to gain an overview of the process while obtaining quantifiable results. This results in speeding up the designing and optimizing processes, while cutting the costs, as the amount of prototypes and experiments will decrease [1].

The simulation presented in this work describes an opening of contacts between which an electric arc is created. This phenomenon is an important part of circuit breakers, which are used to interrupt fault currents. The opening of contacts leads to the formation of an electric arc, which then moves along the electrodes towards an extinguishing area, where the arc is extinguished, and the fault current is finally cut off. A closer description of a circuit breaker can be found in [1, 2].

Apart from designing and optimizing circuit breakers as a safety feature for power systems, general applications of MHD can be found in naval technologies. For example, the US Navy is changing pneumatic and hydraulic devices for electromechanical and also they are replacing traditional weapon systems, which are of chemical and thermodynamic nature, with directed energy and electric weapons. An example of such weapon system is an electromagnetic railgun, which uses the electromagnetic force to accelerate projectiles.

The effects of magnetic fields on electrically conducting fluids can be also used for a power generation. MHD generator is based on the flow of electrically conducting gas through a magnetic field, which generates a voltage [3].

Another interesting application of MHD can be found in pumping conducting fluids (either a saltwater, liquid metal, or an ionized gas) by applying an electromagnetic field. This type of pump can be also used as a propulsion system for spaceships or military submarines [4].

2. Numerical Model

The modelling of plasmas is a very complex process which combines hydrodynamics, thermodynamics and electromagnetics and sometimes even a movement of mechanical parts. There are many different approaches that can be used to describe a plasma phenomenon such as:

- the particle description, which is based on the Lagrangian approach which is characterized by tracking particle trajectories. The position of every particle is calculated at every timestep. The Lagrangian approach uses the immediate application of Newton's laws of the mechanics for physical bodies. It needs to account for all types of species that can be present in a plasma (electrons, all types of ions and neutral particles). From the classical point of view, any particle can be described by its position vector and velocity vector. However, this description is only acceptable for mono-atomic gases, as for the particles of bi-atomic gases, it is necessary to include two additional degrees of freedom for the orientation of the molecule, and other two for the angular velocity of rotation. Although the particle description is simple, the results are conveniently obtained only for a small number of particles, as the computational expensiveness of the problem increases greatly with the number of particles [5],
- the Kinetic description, which is built on the idea of the Boltzmann transport equation. The Boltzmann equation has been initially established for dilute gases of neutral molecules, but it can be also used to describe the evolution of plasmas, which are determined by electron-molecule and ion-molecule collisions.

Two main forms of the Boltzmann equation are used for the description of plasmas. One is collision-less, and the other is collisional which accounts for collisions between particles. Unlike the particle description, which tracks the movement of all particles, the kinetic approach uses a statistical approach based on a particle distribution function:

$$f(\boldsymbol{r},\boldsymbol{v},t)\mathrm{d}\boldsymbol{r}\,\mathrm{d}\boldsymbol{v}\,, \tag{1}$$

which represents the number of particles which at the time t have positions in a space-volume element d$\boldsymbol{r}$ at the magnitude of a position $\boldsymbol{r}$ [m] and velocities lying within a d$\boldsymbol{v}$ element at the magnitude of a velocity $\boldsymbol{v}$ [$\mathrm{m\,s^{-1}}$]. By integrating the particle distribution function over a velocity space, it is possible to get the gas number density. The final form of the Boltzmann equation, which accounts for the electromagnetic force is:

$$\frac{\partial f}{\partial t}+\boldsymbol{v}\cdot\frac{\partial f}{\partial \boldsymbol{r}}+\frac{q(\boldsymbol{E}+\boldsymbol{v}\times\boldsymbol{B})}{m}\cdot\frac{\partial f}{\partial \boldsymbol{v}}=\left(\frac{\partial f}{\partial t}\right)_{\mathrm{coll}}\,, \tag{2}$$

where $\left(\frac{\partial f}{\partial t}\right)_{\mathrm{coll}}$ describes the collision term. Partial derivatives by vectors mean gradient in the case of $\boldsymbol{r}$ and velocity analogue of gradient in the case of $\boldsymbol{v}$. The disadvantage of the Boltzmann equation lies in its inability to solve long-range Coulomb interactions. This approach is an improvement from the particle approach as it can be used for larger scale simulations. But still, to define the position of particles it is necessary to calculate six quantities (one for each component of the position vector and the velocity vector), which results in a large set of equations. For this reason, it is useful to consider the plasma as a fluid consisting of several species [6],

- multi-fluid models consider each species present in the gas as an individual fluid. This means that the momentum and energy equations are solved separately for each ion species and electrons. The advantage of the multi-fluid model is in the simulation of a mass-dependent-asymmetric behaviour. The model also includes electric fields arising from pressure gradients and an ion demagnetization across boundary layers. The disadvantage is that these models are still quite complex, as it is necessary to solve several PDEs, while it is not always convenient to describe the plasma this precisely [7],
- the two-fluid description of plasma is similar to the multi-fluid description. The main difference is that this approach considers only ions and electrons as separate fluids. This approach is very useful for a description of non-equilibrium phenomena, in which the temperature of electrons is different from the temperature of ions. This non-equilibrium is the result of non-equal collisions. The collisions between ions and electrons are less effective due to the unbalanced mass ratio. For this reason, the electrons will keep a higher temperature, while the ions will keep a lower temperature, so individually, they will thermalize faster than the whole plasma as a single fluid. Another part of the non-equilibrium phenomenon is a violation of the quasi-neutrality. The Debye length is a characteristic distance over which electrostatic potentials are screened out or attenuated by a redistribution of charged particles. On scales shorter than the Debye length, microscopic electric fields are non-negligible, and particles interact by Coulomb forces. This violation of the quasi-neutrality

is commonly seen near the electrodes, as the particles with the opposite charge will be accumulated there [8, 9],

- magnetohydrodynamic approach considers a plasma as a single fluid. It is the extension of fluid dynamics to electrically conducting fluids with the inclusion of electromagnetic forces. MHD equations describe the evolution of macroscopic quantities such as the density, the velocity, the pressure and the magnetic field. These models are very useful when the exact motion of particles is not of the interest. The MHD approach considers that the plasma is quasi-neutral, which means the number of electrons and ions is the same, and so the plasma is neutral on scales larger than the Debye length. This also implies $\nabla \cdot \boldsymbol{J} = 0$, which removes most electrostatic instabilities. The MHD approach also assumes that the plasma is in the thermal equilibrium, which means that the temperature of electrons is the same as the temperature of heavy particles. There are few descriptions of MHD based on the form of the magnetic induction equation. The ideal model neglects the source terms in the magnetic induction equation and is only applicable when the heat flow is not important [10]:

$$\frac{\partial \boldsymbol{B}}{\partial t} - \nabla \times (\boldsymbol{v} \times \boldsymbol{B}) = 0 \,. \tag{3}$$

The Hall model includes the Hall effect, which allows the ions and electrons move at different velocities:

$$\frac{\partial \boldsymbol{B}}{\partial t} - \nabla \times (\boldsymbol{v} \times \boldsymbol{B}) = \nabla \times \left(-\frac{\boldsymbol{j}}{nq} \times \boldsymbol{B} \right). \tag{4}$$

The resistive model adds the resistive term to the induction equation along with Joule heating Q_j [W m^{-3}] in the energy equation:

$$\frac{\partial \boldsymbol{B}}{\partial t} - \nabla \times (\boldsymbol{v} \times \boldsymbol{B}) = \nabla \times \left(-\frac{\boldsymbol{j}}{\sigma} \right), \tag{5}$$

$$Q_j = \frac{\boldsymbol{j}^2}{\sigma} \,, \tag{6}$$

where $\boldsymbol{B}$ is the vector of magnetic flux density [T], t is the time [s], $\boldsymbol{v}$ is the velocity vector [m s^{-1}], n is the ion number density [m^{-3}], q is the electric charge [C], σ is the electrical conductivity [S m^{-1}] and $\boldsymbol{j}$ is the current density [A m^{-2}].

2.1. Fluid Dynamics

Fluid dynamics are described by Navier-Stokes equations which consist of mass, momentum and energy conservation equations [11]:

- mass equation:

$$\frac{\partial \rho}{\partial t} + \nabla \cdot (\rho \boldsymbol{v}) = 0 \,, \tag{7}$$

where ρ is the density [kg m^{-3}];

- momentum equation:

$$\frac{\partial(\rho v_i)}{\partial t} + \nabla \cdot (\rho v_i \boldsymbol{v}) = \nabla \cdot (\eta \nabla v_i) - \nabla p + \rho \boldsymbol{g} + S_i , \tag{8}$$

where v_i is the velocity in the i-direction, η is the dynamic viscosity [Pa s], p is the pressure [Pa], $\boldsymbol{g}$ is the gravitational acceleration [m s^{-2}] and S_i describes another source terms. Even though the gravitational force is usually much smaller compared to the other forces acting on laboratory plasmas, it was still considered in the simulation as if it does not increase the complexity of the problem considerably.

- energy equation:

$$\frac{\partial(\rho H)}{\partial t} + \nabla \cdot (\rho H \boldsymbol{v}) = \nabla \cdot \left(\frac{\lambda}{C_p} \nabla H \right) + S_j , \tag{9}$$

where H is the enthalpy [J], λ is the thermal conductivity [W m^{-1}K^{-1}], C_p is the specific heat [J kg^{-1}K^{-1}] and S_j describes another source terms.

Equation of state is described by ideal gas law:

$$pV = nRT , \tag{10}$$

where V is the volume [m^3], n is the number of moles of gas [mol], R is the ideal gas constant [J mol^{-1}K^{-1}]and T is the absolute temperature [K].

2.2. Electromagnetics

Maxwell equations in their general form can be described as [12]:

$$\nabla \times \boldsymbol{E} = -\frac{\partial \boldsymbol{B}}{\partial t} , \tag{11}$$

$$\nabla \times \boldsymbol{B} = \mu_0 \boldsymbol{j} + \frac{1}{c^2} \frac{\partial \boldsymbol{E}}{\partial t} , \tag{12}$$

$$\nabla \cdot \boldsymbol{E} = \frac{\rho}{\varepsilon} , \tag{13}$$

$$\nabla \cdot \boldsymbol{B} = 0 , \tag{14}$$

where $\boldsymbol{E}$ is the vector of electric intensity [V m^{-1}], c is the speed of light [m s^{-1}] and μ_0 is the permeability of the free space [H m^{-1}]. These equations impose two different source terms into the momentum equation and that is the Lorentz force $\boldsymbol{F}_{l(\text{specific})}$:

$$\boldsymbol{F}_{l(\text{specific})} = \boldsymbol{j} \times \boldsymbol{B} , \tag{15}$$

and the electrostatic force $\boldsymbol{F}_{e(\text{specific})}$:

$$\boldsymbol{F}_{e(\text{specific})} = \rho_e \boldsymbol{E} , \tag{16}$$

where ρ_e is the charge density [C m^{-3}].

These equations can be simplified and adjusted into a form, which is more suitable for numerical simulations. For most plasma phenomena, it is possible to reduce the analysis to non-relativistic velocities. With the use of a time t_0 and a length scale l_0, it possible to make estimates of the orders of magnitudes for different terms. First, the magnitude of the electric field is approximated as $E \approx v\,B$ and the magnitude of current

density is approximated as $\mu_0 j = B/l_0$ and then the influence of the displacement current in Eq. (12) can be investigated [12]:

$$\frac{1}{c^2}\left|\frac{\partial \boldsymbol{E}}{\partial t}\right| \approx \frac{\boldsymbol{v}^2}{c^2}\frac{B}{l_0} \ll \left|\nabla \times \boldsymbol{B}\right| \approx \frac{B}{l_0}. \tag{17}$$

This means that the time-dependent term can be neglected and Eq. (12) can be rewritten as:

$$\nabla \times \boldsymbol{B} = \mu_0 \boldsymbol{j}. \tag{18}$$

The assumption of non-relativistic velocities also brings a simplification into forces acting on the electrically conductive fluid (Eq. (15) and Eq. (16)):

$$\rho_e \left|\boldsymbol{E}\right| \approx \frac{\boldsymbol{v}^2}{c^2}\frac{B^2}{\mu_0 l_0} \ll \left|\boldsymbol{j} \times \boldsymbol{B}\right| \approx \frac{B^2}{\mu_0 l_0}. \tag{19}$$

This means that the Lorentz force is considerably larger, and so the electrostatic acceleration (Eq. (16)) can be neglected. The relation between the electric current density and the electric field and the magnetic field can be described by the Ohm's law for moving conducting media:

$$\frac{\boldsymbol{j}}{\sigma} = \boldsymbol{E} + \boldsymbol{v} \times \boldsymbol{B}. \tag{20}$$

After these simplifications, resistive MHD equations (without the energy equation) are described as [13]:

$$\frac{\partial(\rho v_i)}{\partial t} + \nabla \cdot (\rho v_i \boldsymbol{v}) = \nabla \cdot (\eta \nabla v_i) - \nabla p + \rho \boldsymbol{g} + \boldsymbol{j} \times \boldsymbol{B}, \tag{21}$$

$$\frac{\partial \boldsymbol{B}}{\partial t} - \nabla \times (\boldsymbol{v} \times \boldsymbol{B}) = \nabla \times \left(-\frac{\boldsymbol{j}}{\sigma}\right), \tag{22}$$

$$\nabla \cdot \boldsymbol{B} = 0, \tag{23}$$

$$\boldsymbol{j} = \sigma(\boldsymbol{E} + \boldsymbol{v} \times \boldsymbol{B}). \tag{24}$$

The term $\nabla \times \left(-\frac{\boldsymbol{j}}{\sigma}\right)$ in Eq. (22) can be described through the magnetic flux density by applying Eq. (18) as: $\nabla \times \left(-\frac{1}{\sigma\mu_0}\nabla \times \boldsymbol{B}\right)$, which is then adjusted by using a vector calculus identity: $\nabla \times (-\nabla \times \boldsymbol{B}) = \nabla(-\nabla \cdot \boldsymbol{B}) + \nabla^2 \boldsymbol{B}$. After the application of Eq. (23), the dissipative term can be described as:

$$\nabla \times \left(-\frac{\boldsymbol{j}}{\sigma}\right) = \frac{1}{\sigma\mu_0}\nabla^2 \boldsymbol{B}. \tag{25}$$

Instead of the magnetic flux density, a magnetic potential vector can be used for the description of the magnetic field. This transforms the Eq. (22) into the form of the general transport equation. The magnetic flux density is defined as a curl of the vector potential $\boldsymbol{A}$ [V s m^{-1}] [13, 14]:

$$\boldsymbol{B} = \nabla \times \boldsymbol{A} . \tag{26}$$

By applying Eq. (25) and Eq. (26), Eq. (22) is changed into:

$$\nabla \times \frac{\partial \boldsymbol{A}}{\partial t} = \nabla \times \left(\boldsymbol{v} \times \nabla \times \boldsymbol{A} \right) + \frac{1}{\sigma \mu_0} \nabla^2 \left(\nabla \times \boldsymbol{A} \right) . \tag{27}$$

After using a vector calculus identity: $\nabla^2 \left(\nabla \times \boldsymbol{A} \right) = \nabla \times \left(\nabla^2 \boldsymbol{A} \right)$, it is possible to "uncurl" the equation, which results in:

$$\frac{\partial \boldsymbol{A}}{\partial t} = \boldsymbol{v} \times \left(\nabla \times \boldsymbol{A} \right) + \frac{1}{\sigma \mu_0} \nabla^2 \boldsymbol{A} + \nabla \phi , \tag{28}$$

where ϕ is an arbitrary scalar quantity. By using another vector calculus identity: $\boldsymbol{v} \times \left(\nabla \times \boldsymbol{A} \right) = \nabla \left(\boldsymbol{v} \cdot \boldsymbol{A} \right) - \boldsymbol{A} (\boldsymbol{v} \cdot \nabla)$, and fixing the gauge by selecting the value of gradient to: $\nabla \phi = -\left(\boldsymbol{v} \cdot \boldsymbol{A} \right)$, the equation is changed into:

$$\frac{\partial \boldsymbol{A}}{\partial t} = -\left(\boldsymbol{v} \cdot \nabla \right) \boldsymbol{A} + \frac{1}{\sigma \mu_0} \nabla^2 \boldsymbol{A} . \tag{29}$$

3. Simulation and Results

A simulation concerning a contact opening was investigated. Simulations were carried out in ANSYS FLUENT, which is a commercially available CFD (Computational fluid dynamics) software that uses a finite volume method for calculating PDEs (Partial differential equations).

ANSYS FLUENT also includes an MHD add-on module which describes the influence of the electromagnetic field on the fluid flow. This module provides two alternatives for calculating the current density which is featured in the source term in Navier-Stokes equations. First option uses an electric potential φ [V]:

$$\boldsymbol{j} = -\sigma \nabla \varphi . \tag{30}$$

In this method, it is possible to select either a current density or an electric potential as a boundary condition.

An alternative option uses the magnetic flux density:

$$\boldsymbol{j} = \frac{1}{\mu_0} \nabla \times \boldsymbol{B} . \tag{31}$$

This method only uses magnetic flux density boundary conditions, which means it is not usable for a plasma simulation, as it is impossible to define the electric field through the boundary conditions. In conclusion, the built-in MHD model is unable to calculate electric and magnetic fields simultaneously.

ANSYS FLUENT offers a possibility to import new custom models through UDSs (User defined scalars) and UDFs (User defined functions). A UDS is a new quantity for which a general transport equation is solved:

$$\frac{\partial \left(\rho \phi \right)}{\partial t} + \nabla \cdot \left(\boldsymbol{v} \rho \phi - \Gamma \nabla \phi \right) = S_\phi , \tag{32}$$

where $\frac{\partial(\rho\phi)}{\partial t}$ is the unsteady term, $\nabla \cdot \boldsymbol{v}\rho\phi$ is the convective term, $\nabla \cdot (-\Gamma \nabla \phi)$ is the diffusion term and S_ϕ describes a source term, ϕ is an universal scalar quantity and Γ is the diffusion coefficient.

A UDF is a code based on C/C++ language which is used to adjust or to enhance FLUENTs standard features. The code can be imported either through an inbuilt compiler or through Microsoft Visual Studio which can be linked to FLUENT. UDFs are used to customise terms in the transport equation for UDSs, boundary conditions, material properties, the initialisation of solutions or to adjust existing models. For every purpose, there is a pre-defined UDF, which consists of a header starting with a DEFINE term, which is followed by the application of the function and only the body is defined by the user. The advantage of the MHD model is that it can be defined by transport equations of the electric potential and the magnetic vector potential, which were described in the text earlier. As a UDS only describes a scalar quantity, whereas the magnetic vector potential is a vector quantity, it was necessary to create an individual UDS for every component of the magnetic vector potential. In total, four UDS equations, one for the electric potential and three for the magnetic vector potential, were added and solved directly by FLUENT. The magnetic flux density, the electric intensity and the electric current density were calculated from the directly solved quantities. A UDF called DEFINE_SOURCE was used to describe the source terms in transport equations. The function DEFINE_PROPERTY was used to describe material properties. The movement of contacts was defined by DEFINE_CG_MOTION.

3.1. Custom Model

Eq. (29) was used to derive the equations of the vector potential, while Eq. (34) describes the electric field through the electric potential. This set of equations was imported into FLUENT:

$$\frac{\partial A_i}{\partial t} + \nabla \cdot (\boldsymbol{v} A_i) - \frac{1}{\sigma \mu_0} \nabla^2 A_i = 0 , \tag{33}$$

$$\nabla \cdot (\sigma \nabla \varphi) = 0 , \tag{34}$$

with the relation of the dissipative term to the current density being:

$$\frac{1}{\sigma \mu_0} \nabla^2 A_i = -j_i , \tag{35}$$

where A_i is the component of magnetic vector potential in the i-direction and j_i is the component of current density in the i-direction which was described by Eq. (24).

Apart from definitions of the magnetic vector potential and the electric potential, additional source terms describing the effects of the electromagnetic field on the momentum and the energy equation were implemented. The momentum equation source terms consisted of components of the Lorentz force. As for the energy equation, source terms describing the Joule heating and the radiation based on the net emission coefficient were implemented. The values of the net emission coefficient (NEC) ε_N were obtained from [15]. The parameters of the plasma such as the density, the thermal conductivity, the viscosity, the specific heat and the electrical conductivity were obtained from [16].

3.2. Assumptions

To simplify the solution, certain assumptions were made:

- the plasma was considered to be in a local thermodynamic equilibrium (LTE), which is usually used for modelling of thermal plasmas at atmospheric or higher pressures due to high number densities of species, which results in a strong collisional coupling for the energy exchange between electrons and heavy particles. The result of this assumption is a possibility to use one temperature for the description of fluid,
- similar to papers [1, 2], the arc ignition is not included in the simulation and the calculation start with a constant temperature distribution and a small gap between contacts,
- vapours from electrodes and chemical reactions were not taken into account, as the main goal was to implement the MHD model.

Tab. 1 Source terms

Equation	Source term
X-momentum	$j_z B_y - j_y B_z$
Y-momentum	$j_x B_z - j_z B_x$
Z-momentum	$j_y B_x - j_x B_y$
Energy	Joule heating: $\frac{1}{\sigma} j^2$ Radiation: $-4\pi\varepsilon_N$

3.3. Geometry

A simplified 3D geometry which consists of two metal contacts separated by an air region was used. The diameter of contacts was set to 10 mm and the initial distance between contacts was set to 0.1 mm. For a simplification, the geometry of contacts was not considered as it does not affect the solution noticeably.

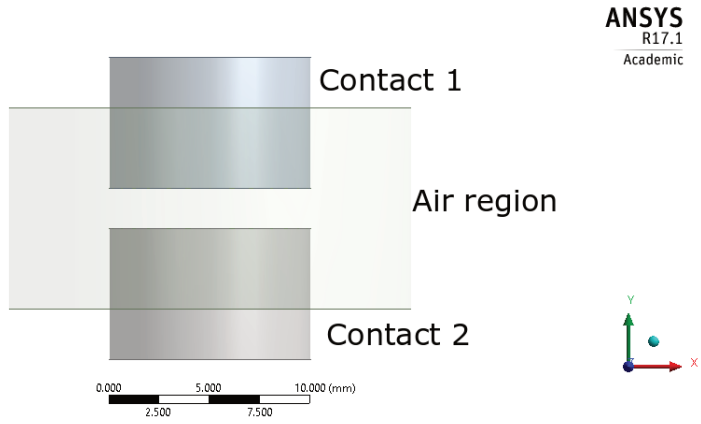

Fig. 1 Simplified 3D geometry

3.4. Solver Settings and Boundary Conditions

A pressure-based solver was used. The type of flow was set to laminar because of assumed low velocity of the fluid. A boundary condition of uniform current density of 250 000 $\mathrm{A\,m^{-2}}$ was imposed on the horizontal (top) wall of the Contact 2 and the boundary condition of a zero electric potential was imposed on the horizontal (bottom) wall of the Contact 1. Side walls of contacts were set as insulating walls. The thermal boundary condition of zero heat flux was set to contact walls. This boundary condition ensured that no heat would leave the system through contact walls which helped with keeping a temperature and, as a result, a high electrical conductivity near the contacts. The high electrical conductivity is necessary to maintain the connection of the arc with the contact. Outer walls of the air region were set as a pressure outlet with a defined constant atmospheric pressure. The temperature of the backflow was set to 300 K, so the temperature in the region would not increase constantly. Simulations were carried out as transient with a timestep of 1 μs. For the pressure-velocity coupling, a coupled method was used, as it helped with the stability of the solver and opened the option to select the Courant number, which was set to one. A second-order upwind method was used for spatial discretization.

Tab. 2 Boundary conditions

Boundary	Thermal	Electric	Motion	Vector potential
Top contact	$\frac{\partial T}{\partial \boldsymbol{n}} = 0$	$\varphi = 0\ \mathrm{V}$	$v_y = 1\ \mathrm{ms^{-1}}$	$\boldsymbol{A} = 0$
Bottom contact	$\frac{\partial T}{\partial \boldsymbol{n}} = 0$	$j = 250\,000\ \mathrm{Am^{-2}}$	$v_y = -1\ \mathrm{ms^{-1}}$	$\boldsymbol{A} = 0$
Walls of the air region	Backflow $T = 300\ \mathrm{K}$	$\frac{\partial \varphi}{\partial \boldsymbol{n}} = 0$		$\frac{\partial \boldsymbol{A}}{\partial \boldsymbol{n}} = 0$

4. Results

A comparison of the built-in and the presented model was carried out. Without any adjustments, it would not be possible to properly carry out a simulation with the built-in model, as the radiation plays an important part in plasma phenomena, and so the radiation model had to be added. The main difference between these models was that the presented model accounted for the effects of magnetic field on the plasma through the Lorentz force. The results from these simulations were comparable, as the arc temperature stabilized at approximately 13 500-14 000 K, which lasted till the breakdown of the arc. The arc broke down at slightly similar times (2.4 ms for the presented model and around 2.5 ms for the built-in model). In the custom model, it was possible to see a slight decline of temperature which was caused by a slightly larger movement of the arc. The temperature evolutions at the centre of the arc are shown in Figs 2, 3.

Next figures display the temperature distribution of the arc calculated by the presented custom model. As the transient behaviour of the arc calculated by the built-in and the presented model was similar, only the results from the presented model are shown here. The only significant difference was in bending of the arc (see Fig. 6). In the built-in model, the arc bent to the other side. Figs 4, 5 and 6 show a sharp transi-

tion of the temperature at the edge of the plasma column while only a slight variation is visible inside the column.

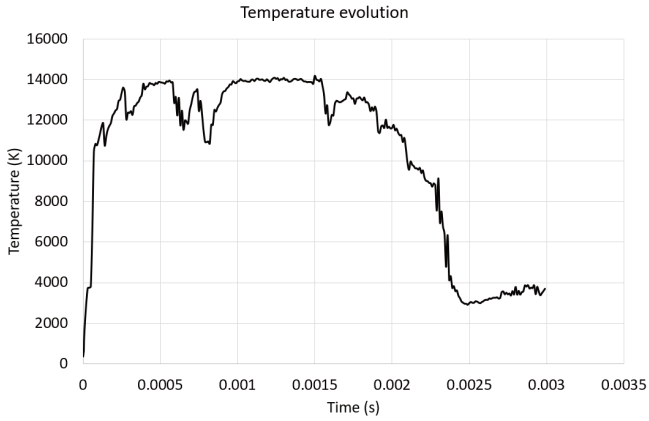

Fig. 2 Temperature evolution of the built-in MHD model

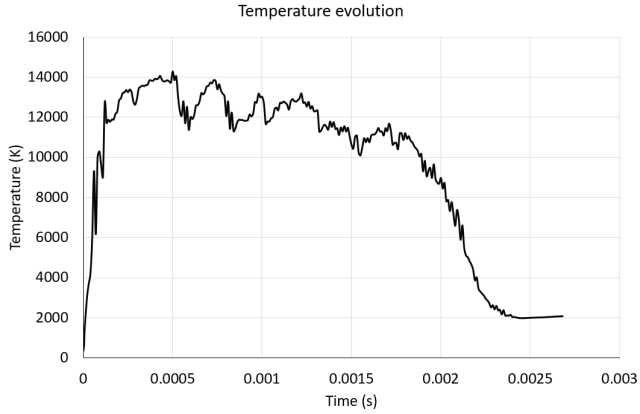

Fig. 3 Temperature evolution of the custom MHD model

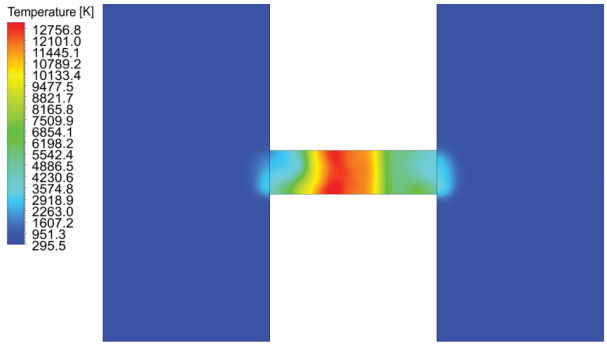

Fig. 4 Temperature distribution at time t = 0.0006 s

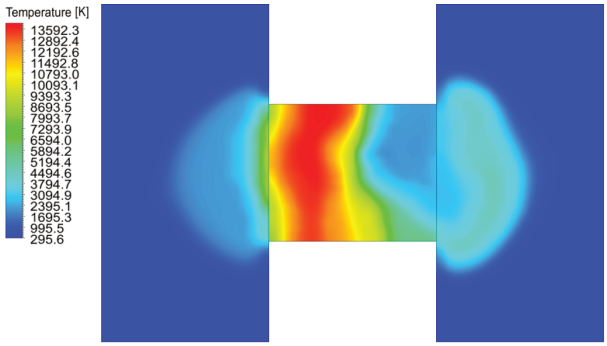

Fig. 5 Temperature distribution at time t = 0.002 s

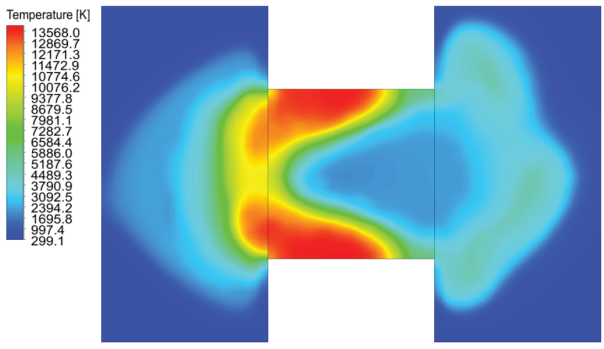

Fig. 6 Temperature distribution at time t = 0.0025 s

The investigation of the magnetic field was focused on the effects and not on the time evolution, so the results are shown only for one timestep in which the distance between the contacts was 5 mm. Fig. 8 shows components of the magnetic flux density which represents the circulation of the magnetic field. The results correspond with Maxwell equations and Eq. (18) and Eq. (26). Inside the plasma arc, there was a very small magnetic flux density, which then increased in the outward direction. The maximum value of the magnetic flux density has been reached at the edge of the plasma column. The horizontal distribution was not uniform, as the value of magnetic flux density (12.189 μT) near the electrodes was higher than the value in the centre (5.037 μT). The slight movement of the arc did not seem to significantly affect the magnetic field.

5. Discussion

This study investigated numerical modelling of thermal plasmas based on MHD. A model for non-relativistic velocities was derived from the Maxwell equations. The magnetic induction equation was then transformed to a vector potential form which is more suitable for numerical simulations, as it has a form of the transport equation and a simple definition of its source terms. For the temperatures higher than approximately 5 000 K, it is necessary to include a radiation model as the radiation becomes an important part in energy distribution. The most common model used in plasma simulations is a model based on NEC.

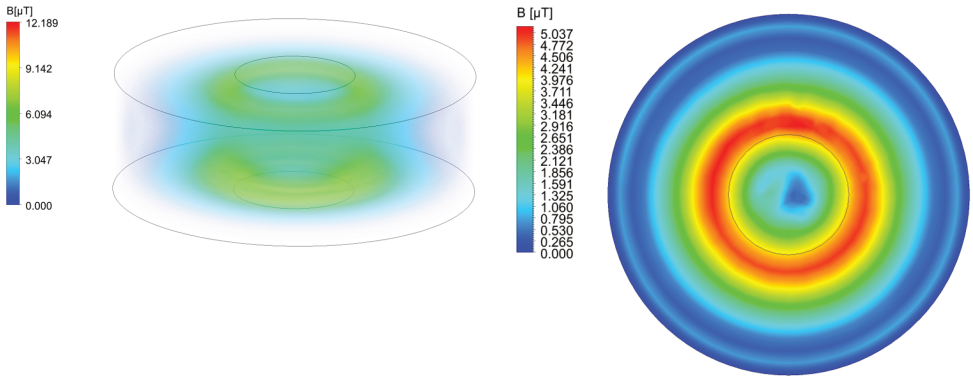

Fig. 7 The magnitude of the magnetic flux density in 3D (left side) and in a 2D cut (right side) which is situated in the middle between the contacts

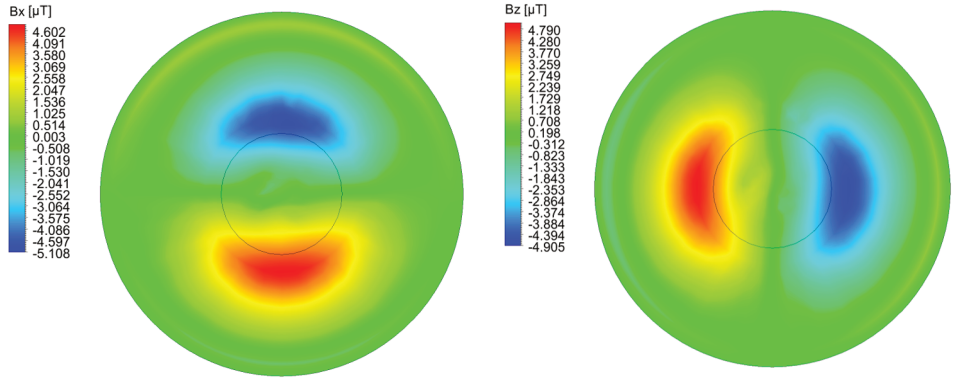

Fig. 8 Components of the magnetic flux density in the x direction (left side) and in the z direction (right side)

Early versions of simulations applied a lower current density which resulted in a lower temperature of the electric arc. In those cases, the arc temperature was around 5 000 K, which was the reason of a completely symmetric arc, as the Lorentz force was negligible, and the material properties of the fluid did not vary considerably. The current density was then increased so the whole phenomenon could be captured.

Even in the present case, the arc was symmetrical during low temperatures. As soon as the mentioned temperature of approximately 5 000 K has been surpassed, there was a sudden change in the shape of the arc, as the material properties changed significantly, and the arc started to display a stochastic nature. The solution converged as expected, nevertheless this change in the shape of the arc should still be examined further.

With the increasing distance between the contacts, the arc started to bend into a certain direction. The bending was most likely the result of boundary conditions at the walls of the air region. As the gas expanded in the arc, the pressure outlet ensured a flow out of the region and so the arc bent in the direction of the flow. The possible solution to this problem is to change the boundary condition from a pressure outlet to

a wall with constant temperature. Also, a small vent should be created, so the pressure inside the region wouldn't increase constantly.

In this case, the Lorentz force does not affect the movement of the arc significantly. To properly see the differences between these models, it would be necessary to change the geometry to allow a larger movement of the arc, increase the current density or use an alternating current with high frequency. This means that in a case of a low velocity of the plasma or a low current density, it is not always necessary to resolve the magnetic field, as the field will not affect the accuracy of the results. From the simulations it is possible to conclude that the custom MHD model resembles the built-in model. While the simulations showed promising results, it would be beneficial to compare the results with real experiments, which could lead to possible adjustments. Still, the model can be used as a base for the next research in plasma dynamics or generally for magnetohydrodynamic simulations.

The description of electromagnetic field used in MHD might be also useful for coupled simulations in electron microscopy. As these phenomena occur in a vacuum, the electromagnetic field cannot affect any flow, but these equations can be used for modelling electromagnetic coils directly in FLUENT by defining a current density condition inside solid regions of coils. This means, that there would be no need for exporting the magnetic field data from MAXWELL to FLUENT. A second application might be found in directly investigating electromagnetic fields created by electrons. As electrons are charged particles, they create an electric field and by their movement they also create a magnetic field. This means it would be possible to investigate the effects of these fields on electrons and investigate induced fields in surroundings.

Acknowledgement

This work was supported by BUT specific research programme (project No. FEKT-S-17-4595).

References

[1] WU, Y., RONG, M., LI, X., MURPHY, A.B., WANG, X., YANG, F. and SUN, Z. Numerical Analysis of the Effect of the Chamber Width and Outlet Area on the Motion of an Air Arc Plasma. *IEEE Transactions on Plasma Science*, 2008, vol. 36, no. 5, p. 2831-2837. DOI 10.1109/TPS.2008.2004040.

[2] YANG, F., WU, Y., RONG, M., SUN, H., MURPHY, A.B., REN, Z. and NIU, C. Low-voltage Circuit Breaker Arcs–Simulation and Measurements. *Journal of Physics D: Applied Physics*, 2013, vol. 46, no. 27, paper 273001. DOI 10.1088/0022-3727/46/27/273001.

[3] BEACH, F.C. and McNAB I.R. Present and Future Naval Applications for Pulsed Power. In *Proceedings of the IEEE Pulsed Power Conference*. Monterey: IEEE, 2005, p. 1-7. DOI 10.1109/PPC.2005.300462.

[4] AL-HABAHBEH, O.M., AL-SAQQA, M., SAFI, M. and ABO KHATER, T. Review of Magnetohydrodynamic Pump Applications. *Alexandria Engineering Journal*, 2016, vol. 55, no. 2, p. 1347-1358. DOI 10.1016/j.aej.2016.03.001.

[5] GHEZZI, L. and BALESTRERO A. *Modeling and Simulation of Low Voltage Arcs*. [PhD thesis]. Delft: Delft University of Technology, 2010, 348 p.

[6] LOUREIRO, J. and AMORIM, J. *Kinetics and Spectroscopy of Low Temperature Plasmas*. Cham: Springer International Publishing, 2016, 441 p. ISBN 978-3-319-09253-9.

[7] KALLIO, E., CHAUFRAY, J., MODOLO, R., SNOWDEN, D. and WINGLEE, R. Modeling of Venus, Mars, and Titan. *Space Science Reviews*, 2011, vol. 162, no. 1-4, p. 267-307. DOI 10.1007/s11214-011-9814-8.

[8] BURBY, J.W. Magnetohydrodynamic Motion of a Two-fluid Plasma. *Physics of Plasmas*, 2017, vol. 24, no. 8, paper 082104. DOI 10.1063/1.4994068.

[9] STENSON, E.V., HORN-STANJA, J., STONEKING, M.R. and PEDERSEN, T.S. Debye Length and Plasma Skin Depth: Two Length Scales of Interest in the Creation and Diagnosis of Laboratory Pair Plasmas. *Journal of Plasma Physics*, 2017, vol. 83, no. 1, paper 595830106. DOI 10.1017/S0022377817000022.

[10] LEDVINA, S.A., MA, Y.J. and KALLIO E. Modeling and Simulating Flowing Plasmas and Related Phenomena. *Space Science Reviews*, 2008, vol. 139, no. 1-4, p. 143-189. DOI 10.1007/s11214-008-9384-6.

[11] VYROUBAL, P., MAXA, J., NEDĚLA V., JIRÁK J. and HLADKÁ, K. Apertures with Laval Nozzle and Circular Orifice in Secondary Electron Detector for Environmental Scanning Electron Microscope. *Advances in Military Technology*, 2013, vol. 8, no. 1, p. 59-69. ISSN 1802-2308.

[12] GOEDBLOED, J.P. and POEDTS, S. *Principles of Magnetohydrodynamics: with Applications to Laboratory and Astrophysical Plasmas*. New York: Cambridge University Press, 2004, 607 p. ISBN 978-0-521-62347-6.

[13] BEN SALAH, N., SOULAIMANI, A. and HABASHI, W.G. A Finite Element Method for Magnetohydrodynamics. *Computer Methods in Applied Mechanics and Engineering*, 2001, vol. 190, no. 43-44, p. 5867-5892. DOI 10.1016/S0045-7825(01)00196-7.

[14] PRICE, D.J. Smoothed Particle Hydrodynamics and Magnetohydrodynamics. *Journal of Computational Physics*, 2012, vol. 231, no. 3, p. 759-794. DOI 10.1016/j.jcp.2010.12.011.

[15] BILLOUX, T., CRESSAULT, Y., TEULET, P. and GLEIZES, A. Calculation of the Net Emission Coefficient of an Air Thermal Plasma at Very High Pressure. *Journal of Physics: Conference Series*, 2012, vol. 406, paper 012010. DOI 10.1088/1742-6596/406/1/012010.

[16] MURPHY, A.B. Transport Coefficients of Air, Argon-Air, Nitrogen-Air, and Oxygen-Air Plasmas. *Plasma Chemistry and Plasma Processing*, 1995, vol. 15, no. 2, p. 279-307. DOI 10.1007/BF01459700.